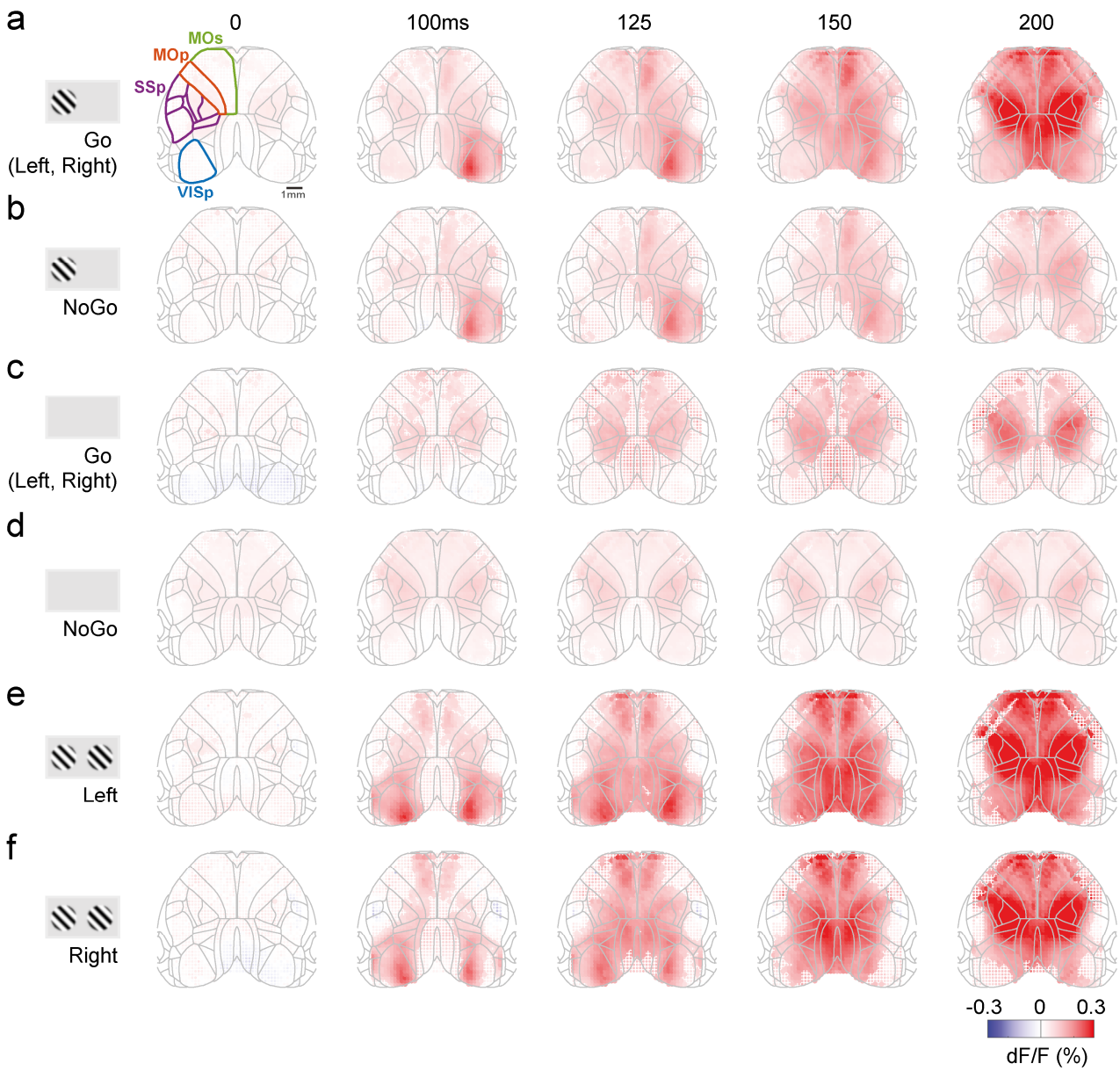


**Supplementary Figure S1: Average cortical fluorescence (dF/F) for different task conditions.**
**(a)** Timecourse of cortical fluorescence, averaged over Go trials (Left or Right choice), with positive contrast present on the left side, and zero contrast on the right. Columns indicate successive time steps after stimulus onset. Each map is overlaid with an outline of cortical regions defined by the Allen CCF, and widefield fluorescence is cropped to the outer edges. Four different cortical regions are highlighted in the left panel (VISp, SSp, MOp, MOs). Maps are averaged over 39 sessions in 9 mice, with dot size indicating significance across sessions ($p$<0.001; nested ANOVA). Even though the animal turns the wheel, the stimulus does not move on the screen in this time period (see Supplementary Figure S2a). **(b)** Average cortical fluorescence for NoGo trials with positive contrast on the left screen. The maps in (a) and (b) are averaged over trials with matched contrast values **(c)** Average cortical fluorescence for Go trials (Left or Right choice) with zero contrast on both sides. **(d)** Average cortical fluorescence for NoGo trials with zero contrast on both sides. **(e)** Average cortical fluorescence for Left choice trials with equal non-zero contrast on both screens. **(f)** Average cortical fluorescence for Right choice trials with equal non-zero contrast on both screens, and mice made a Right choice. The maps in (e) and (f) are averaged over trials with matched contrast values.

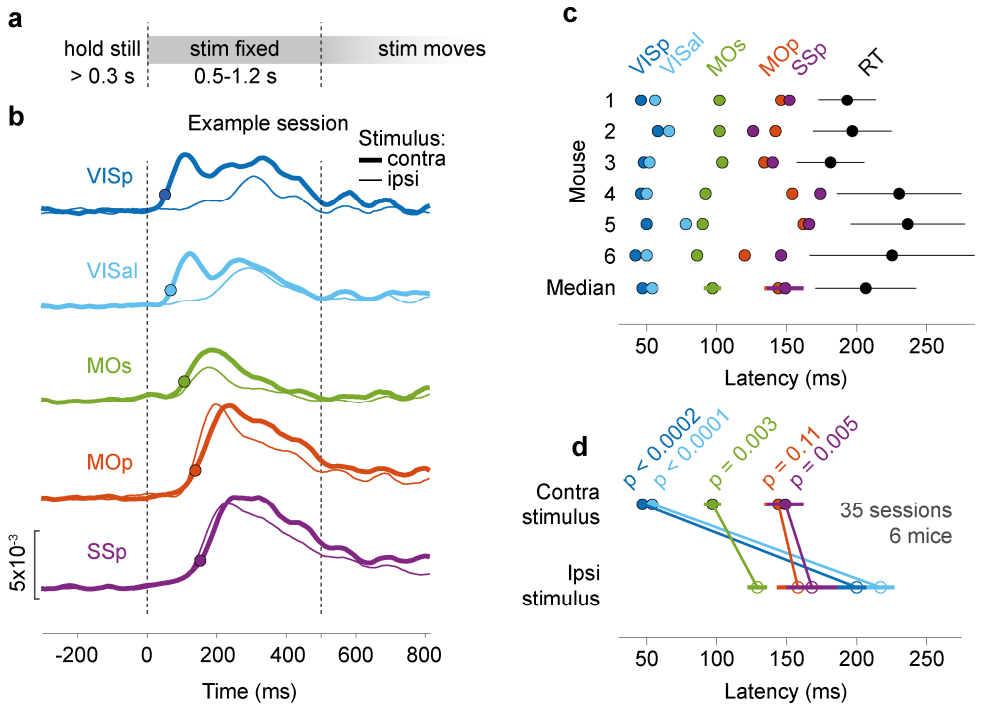


**Supplementary Figure S2: Widefield sequential activation.**

**(a)** Task timeline during widefield calcium imaging. To distinguish activity associated with initial wheel movement from activity driven by visual motion, we introduced an open-loop period 0.5-1.2 s after grating onset, when wheel movements did not move the grating. Trials were excluded post-hoc if choices were made after this period. **(b)** Stimulus-locked calcium fluorescence at 5 ROIs for one example session. Thick lines are the average response to correct trials with only contralateral stimuli. Thin lines are the same but for correct trials with only ipsilateral stimuli. Response latency, marked with a dot, is defined as the time for the mean fluorescence across trials to reach 30% of the peak. **(c)** Summary of fluorescence response latencies to contralateral stimuli for 6 mice (see Methods for genotype information; 3 mice were excluded due to having too few trials to reliably measure onset latency). Rows show data from individual mice, with dots showing each ROI's response latency for trials pooled across sessions. Bottom row: response latencies and reaction time averaged across mice (dots and lines: median ± m.a.d.). **(d)** Response latencies to contralateral and ipsilateral stimuli for each region, averaged across mice (closed and open circles). Significance was determined by a two-tailed paired t-test, t(5)=-10.38, -12.00, -5.46, -1.97, -4.72. Colors as in (b).

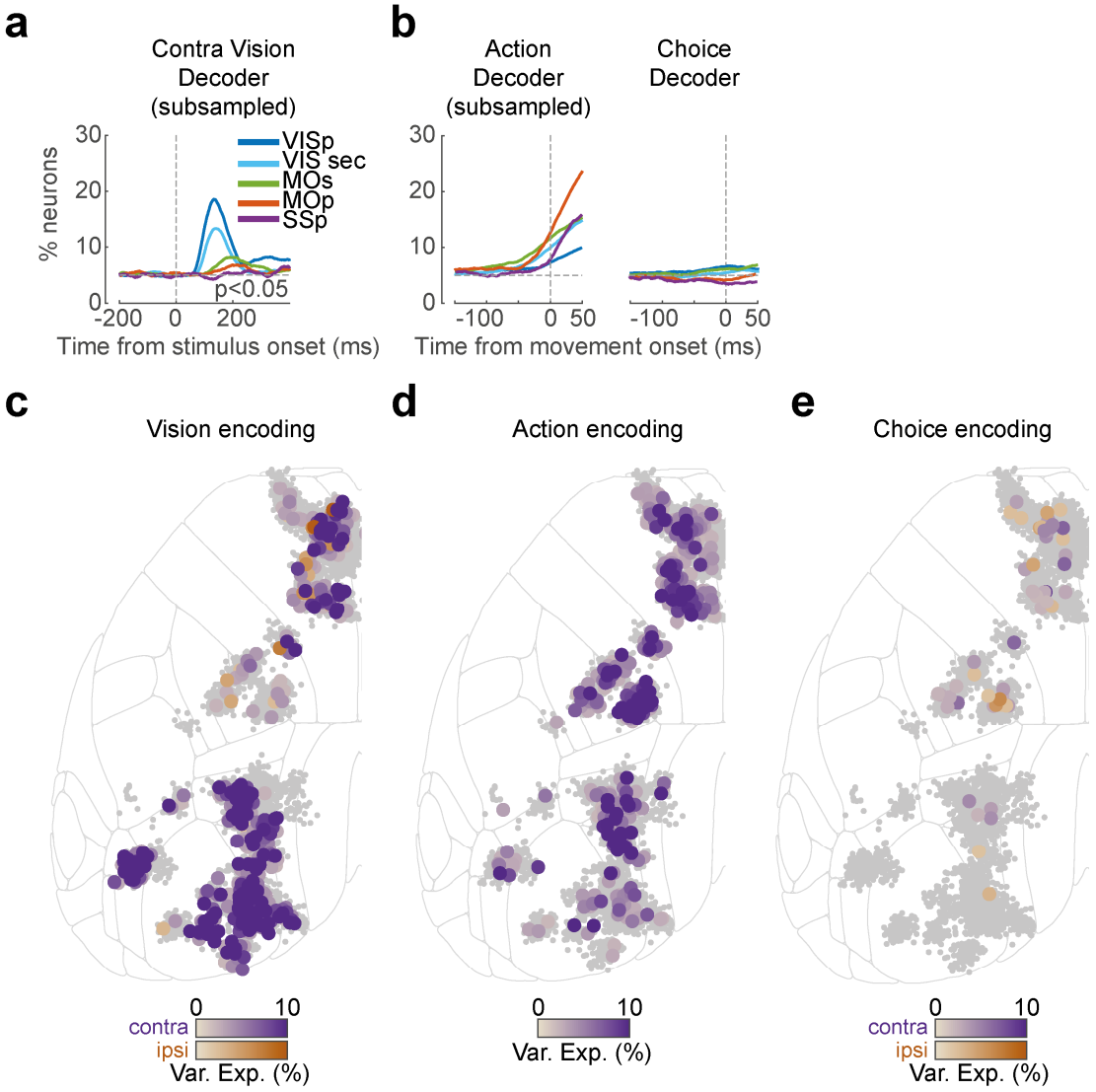


**Supplementary Figure S3: Decoding analysis**

**(a,b)** Same CCCP decoding results as in Fig. 2m-p but using a subsampled number of trials to match with the choice decoder. **(c)** Enlarged version of Fig. 2j, showing single neurons with significant cross-validated variance explained using a contralateral (purple) or ipsilateral (orange) stimulus kernel. **(d)** Enlarged version of Fig. 2k, showing single neurons with significant movement kernels **(e)** Enlarged version of Fig. 2l, showing single neurons with significant kernels for contralateral (purple) or ipsilateral (orange) choice.

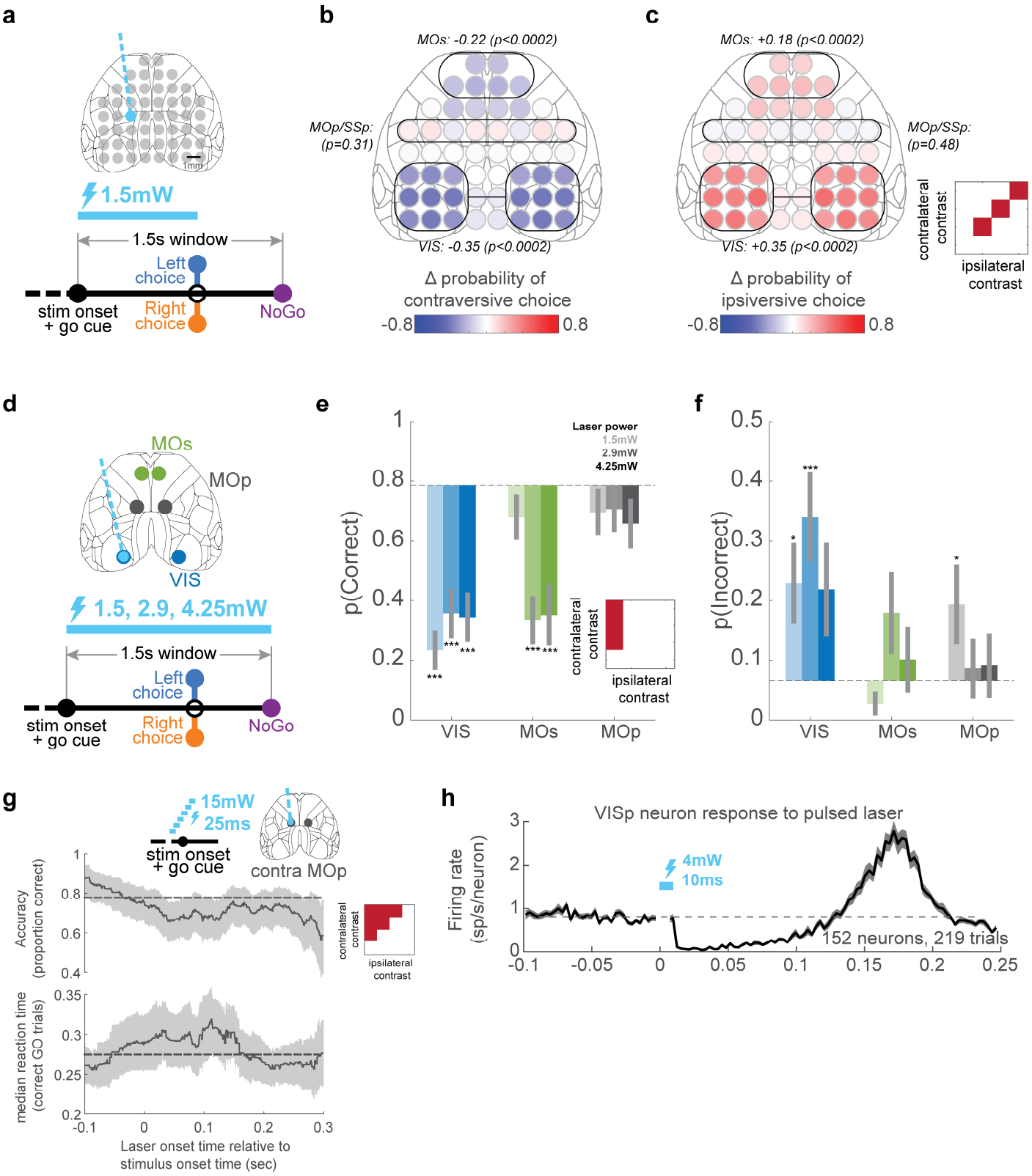


**Supplementary Figure S4: Optogenetic inactivation.**

**(a)** Schematic of the 52-coordinate inactivation experiment. On ~75% of trials, a laser (473 nm, 40 Hz, 1.5 mW) was switched on during stimulus presentation and ceased when a choice (or NoGo) was registered. The location of the laser varied randomly trial-to-trial over 52 cortical sites. **(b)** Summary map of the effect of laser inactivation on contraversive choices, on trials with equal non-zero contrast on each side. Colors indicate the change in the probability of making a contraversive

choice (Left choices for inactivation of right hemisphere locations, and Right choices for left hemisphere locations), averaged across 91 sessions in 5 mice. Data are plotted symmetrically across the hemispheres. Black lines mark regions for which statistical significance was assessed (black italic text), by pooling these regions and shuffling the identities of laser and non-laser trials within each session. **(c)** Summary map of inactivation effect on ipsiversive choices, plotted as in (b). **(d)** Schematic of mixed-power fixed-duration inactivation, focused on VIS, MOs and MOp. Inactivation was performed at several laser powers (1.5, 2.9, 4.25 mW), and the inactivation duration was fixed at 1.5 s, starting at visual stimulus onset. **(e)** Probability of choosing the correct side on trials with visual stimuli present only on one side. The dashed grey line represents the session-averaged non-laser probability of moving to the correct side. Bar values represent the session-averaged probability on trials when inactivating the contralateral VIS (blue), MOs (green) and MOp (dark grey) at laser powers 1.5, 2.9, and 4.25 mW (color intensities; shown inset). Error bars indicate s.e. across sessions. Statistical significance was determined for each subject (pooling data across sessions) using Fisher's exact test, and significance across subjects was determined using Fisher's combined probability test, *** $p<0.001$, ** $p<0.01$, * $p<0.05$. **(f)** As in (e) but plotting the probability of choosing the incorrect side. **(g)** Pulse inactivation experiment in MOp. The onset time of the laser (25 ms, 15 mW) was chosen randomly between -100 ms and +300 ms relative to stimulus onset. Middle: performance is plotted as a function of laser onset time relative to stimulus onset. Data is smoothed with a 100 ms boxcar window. Dashed grey line is the non-laser performance. Bottom: Effect on reaction time for correct Go choices. **(h)** Firing rate of 152 broad-spiking VISp neurons measured electrophysiologically, following a local laser pulse (4 mW 10 ms), in an awake mouse (Ai32 x PV-cre) not performing a task. The period during the light pulse is masked because recorded voltage deflections during this period may have corresponded to light artifacts. Error bars represent s.e.m. across 219 trials.

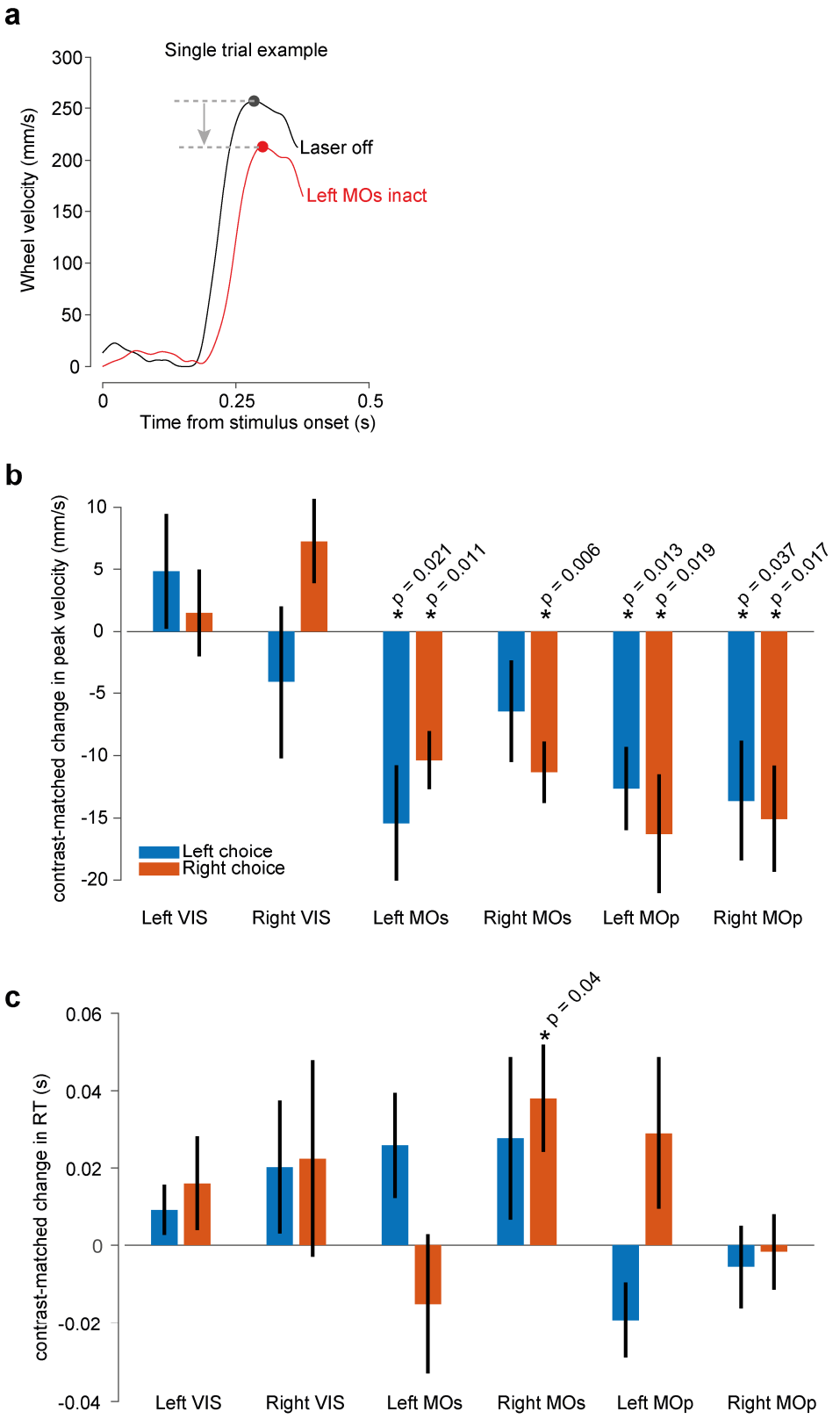


**Supplementary Figure S5: Effect of optogenetic inactivation on wheel peak velocity and reaction time.**
**(a)** Single-trial example of peak velocity change from laser inactivation. Wheel velocity is plotted for a Left choice aligned to stimulus onset for one trial with laser off (black) and laser on in left MOs (red). Peak velocity is indicated with a dot, and a decrease in peak velocity is illustrated by the arrow. **(b)** Summary of the change in peak velocity for Left (blue) and Right (orange) choices, for inactivation in VIS, MOs and MOp in left or right hemispheres (text under plot indicates inactivated region). For each choice and region inactivated, the change in peak velocity is computed within each contrast condition and

then averaged across conditions. Bars indicate the average change in peak velocity and error bars indicate the standard error across subjects. Significance is determined by a t-test and significant $p$ values ($p<0.05$) are shown in the figure. **(c)** Same analysis as in (b) but showing the change in reaction time for Left and Right choices.

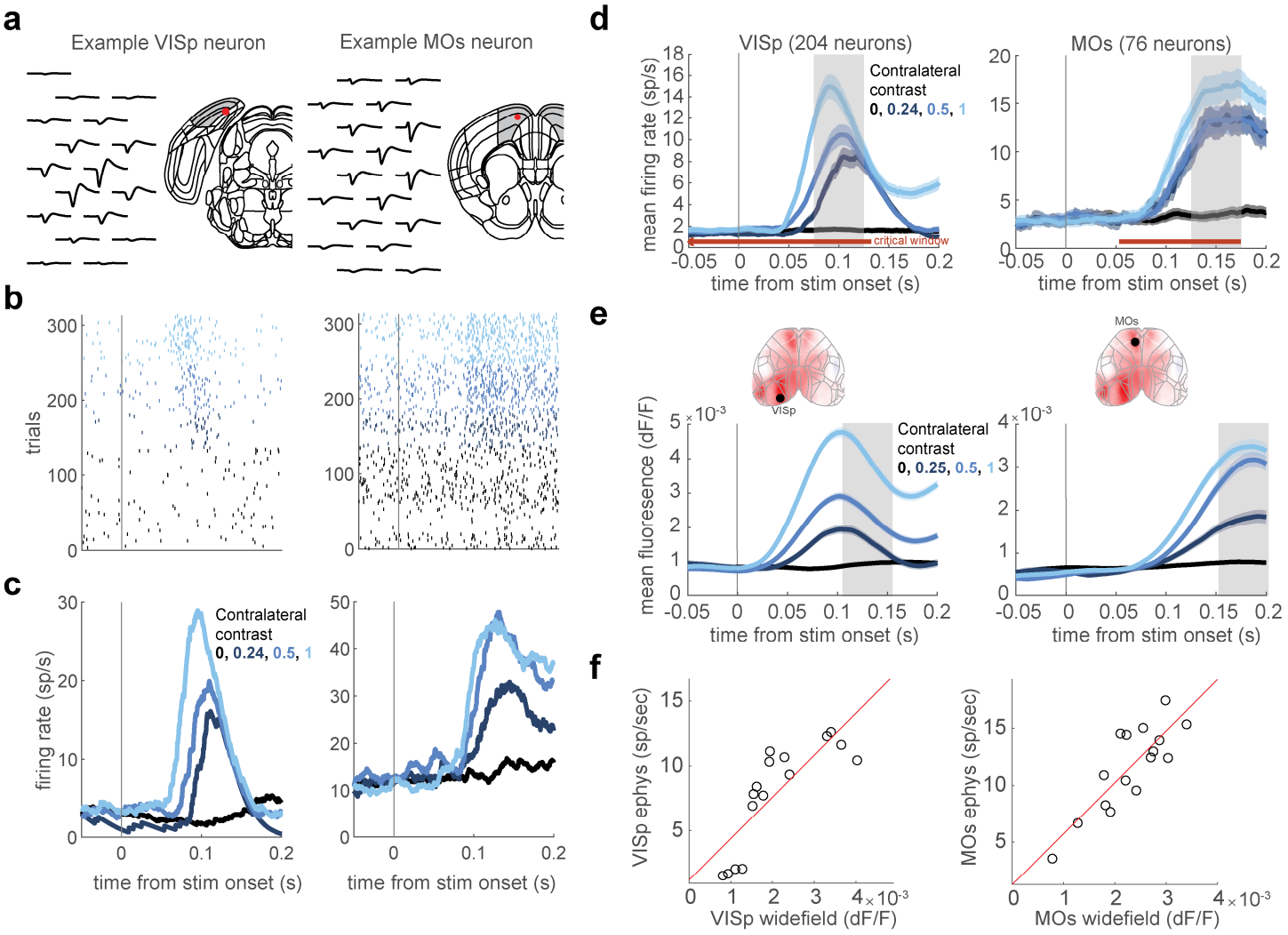


**Supplementary Figure S6: Calibrating widefield activity to spike rate**

**(a)** Example neuron in Left VISp and Left MOs measured electrophysiologically. Mean waveforms are shown in black and the red dot marks the location of the neuron within an aligned Allen CCF atlas. **(b)** Raster plots showing spiking activity aligned to stimulus onset. Color reflects the contrast level presented to the contralateral hemifield (color code in panel c). **(c)** PSTHs for these example neurons. **(d)** Population PSTHs, averaged over 204 neurons in VISp and 76 neurons in MOs. Shaded color region marks the standard error across trials. The gray shaded regions mark the time window when the firing rate is averaged for subsequent analyses (VISp: 75-125ms, MOs: 125-175ms). Horizontal red line marks the time of the critical interval identified in the pulse inactivation experiment (Fig. 3h). **(e)** Same plotting convention as in (d) but showing trial-averaged widefield calcium fluorescence of Left VISp (Left) and Left MOs (right) ROIs in response to stimuli present on the contralateral side. Shaded regions mark the intervals used for averaging in subsequent analyses. This window is 30 ms after the window associated with electrophysiological data, to compensate for the slower kinetics of GCaMP6. Insets: ROI locations superimposed on mean fluorescence at 150 ms after stimulus onset. **(f)** Mean calcium fluorescence vs. population firing rates for Left VISp (left) and Left MOs (right). The 16 open circles correspond to the 16 contrast conditions. Red line corresponds to the fit of a simple linear model f(x) = b0 + b1*x. The linear model is used to transform widefield fluorescence data into estimates of population firing rate in the neurometric model (Fig. 4).

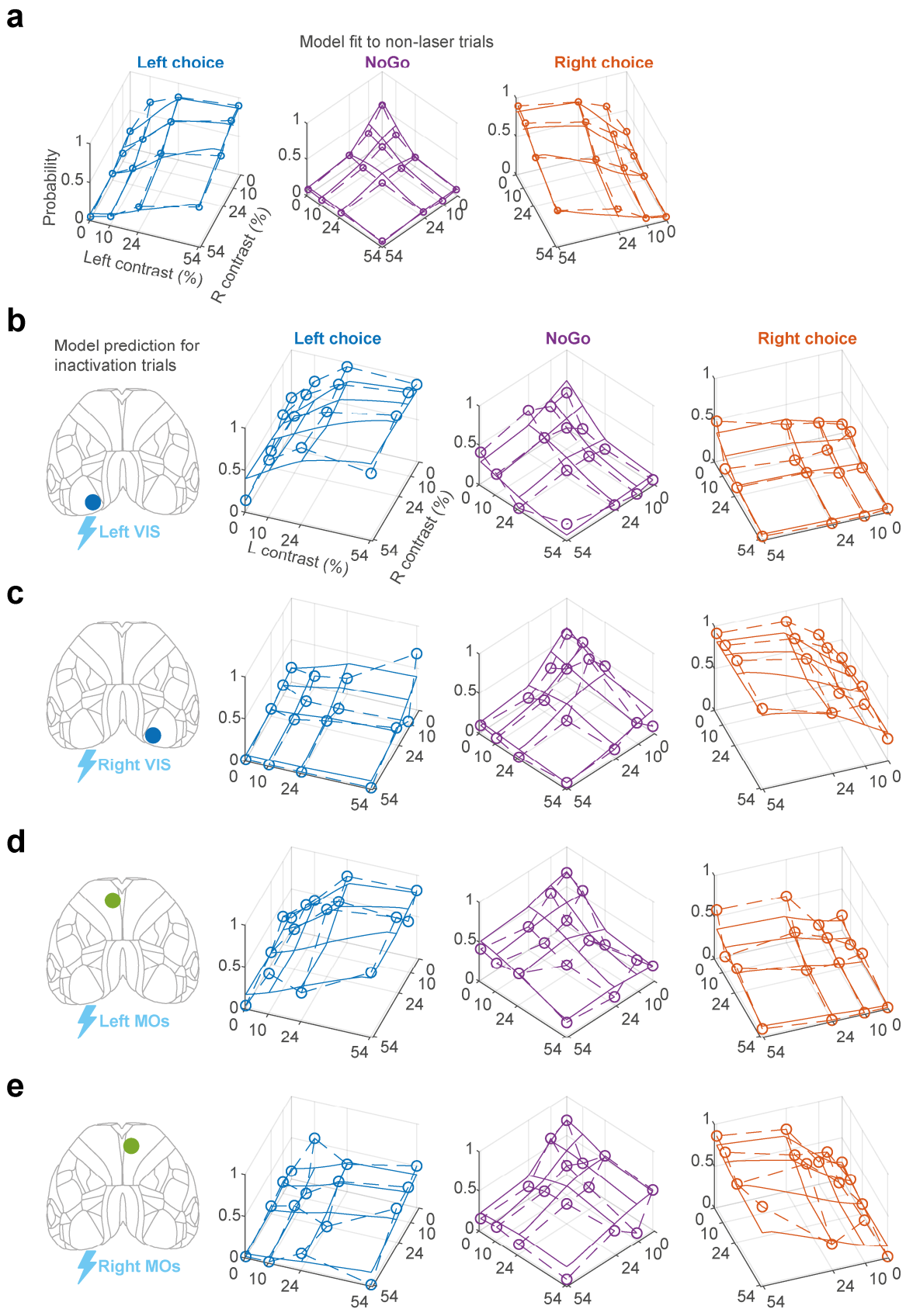


**Supplementary Figure S7: Neurometric model fit and prediction**

**(a)** Fit of the neurometric model to non-laser trials from the mixed-power inactivation sessions, showing all contrast conditions on the left and right side. Same plotting scheme as in Fig. 1e-g. Empirical data are represented as colored dots for Left (blue), NoGo (purple) and Right (orange) choices, averaged across 34 sessions in 6 mice. Solid lines correspond to

the posterior mean of the neurometric model fit. For each contrast condition, the probability of Left, NoGo and Right are computed using the fitted weights and average firing rate for each contrast condition (Supplementary Figure S6) with interpolation between the contrast values tested. **(b-e)** Same plotting scheme as in (a) but showing the data and the prediction of the neurometric model when inactivating Left VIS (b), Right VIS (c), Left MOs (d) and Right MOs (e) for 1.5 s from stimulus onset, averaged over all laser powers. Model predictions are generated by setting the activity for each region to zero in the model.

[Supplementary Movie 1]

**Supplementary Movie 1: Widefield fluorescence in VISp, MOs, MOp/SSp for different contralateral and ipsilateral contrast conditions.**

Each panel shows the timecourse of fluorescence in one cortical region, for all 16 contrast conditions. Within each panel, the two black grids show the 40th and 60th percentile (across sessions) of widefield fluorescence (dF/F), averaged over all possible behavioral choices. Different frames of the movie correspond to different times after stimulus onset. Time is indicated in the title of each panel.

[Supplementary Movie 2]

**Supplementary Movie 2: Average widefield fluorescence in VISp, MOs, MOp/SSp for different contralateral and ipsilateral contrast conditions, and choices.**

Similar to Supplementary Movie 1, but dividing responses by behavioral choice. The three grids in each panel show mean cortical fluorescence as a function of contrast condition, separated for Contraversive (away from the ROI hemisphere; blue), NoGo (purple) and Ipsiversive (towards the ROI hemisphere; orange) choices. Conditions where there are fewer than 0.5 trials averaged across sessions (e.g. trials with high contrast on one side but the mouse moved the opposite direction) are excluded from plotting.

| | | | Session number for each Figure | | | | |
|---|---|---|---|---|---|---|---|
| **Name** | **Sex** | **Genotype** | **Fig. 2a-h** | **Fig. 2i-p *** | **Fig. 3a,d** | **Fig. 3g,h** | **Fig. 1e-h Fig. 4c,d** |
| Beadle | M | Ai32 x PV-Cre | | | | 4 | 5 |
| Bovet | M | Ai32 x PV-Cre | | | | 5 | 5 |
| Burnet | M | Ai32 x PV-Cre | | | | 14 | 4 |
| Kornberg | M | Ai32 x PV-Cre | | | | 14 | 8 |
| Medawar | M | Ai32 x PV-Cre | | | | 14 | 4 |
| Ochoa | M | Ai32 x PV-Cre | | | | 14 | 8 |
| Chomsky | F | Ai32 x PV-Cre | | | 16 | | |
| Morgan | F | Ai32 x PV-Cre | | | 8 | | |
| Murphy | M | Ai32 x PV-Cre | | | 28 | | |
| Spemann | M | Ai32 x PV-Cre | | | 26 | | |
| Whipple | F | Ai32 x PV-Cre | | | 13 | | |
| Kendall | F | Ai95 x VGlut1-Cre | 2 | | | | |
| Moniz | M | Ai95 x VGlut1-Cre | 9 | 3 | | | |
| Muller | F | Ai95 x VGlut1-Cre | 1 | 3 | | | |
| Theiler | F | Ai95 x VGlut1-Cre | 1 | 1 | | | |
| Forssman | M | C57BL/6J | | 4 | | | |
| Richards | M | C57BL/6J | | 5 | | | |
| Chain | M | Snap25-GCaMP6s | 4 | | | | |
| Radnitz | F | Snap25-GCaMP6s | 6 | 5 | | | |
| Cori | F | tetO-G6s x CaMK2a-tTA | 6 | 3 | | | |
| Hench | M | tetO-G6s x CaMK2a-tTA | 7 | 4 | | | |
| Reichstein | M | tetO-G6s x CaMK2a-tTA | 3 | | | | |
| Lederberg | F | Vglut1-IRES2-Cre-D | | 7 | | | |
| Tatum | F | Vglut1-IRES2-Cre-D | | 4 | | | |

* Previously published[6]

**Supplementary Table 1: Mouse genotype and session numbers for each figure**